Geomechanics and Engineering, *Vol. 22, No. 3 (2020) 265-275*
DOI: https://doi.org/10.12989/gae.2020.22.3.265

On determining seismic anchor force of anchoring frame structure supporting three-stage slope

Yu-liang Lin*[1,3,4], Li Lu[1a], Ying-xin Li[1b], Yuan Xue[2c], Zhi-jun Feng[2d], Zhi-meng Wang[2e] and Guo-lin Yang[1f]

[1]*School of Civil Engineering, Central South University, Changsha 410075, China*
[2]*China Railway Eryuan Engineering Group Co. Ltd., Chengdu 610031, China*
[3]*MOE Key Laboratory of Engineering Structures of Heavy Haul Railway, Central South University, Changsha 410075, China*
[4]*Joint International Research Laboratory of Key Technology for Rail Traffic Safety, Central South University, Changsha 410075, China*

(Received March 3, 2020, Revised June 22, 2020, Accepted July 6, 2020)

Abstract. As a flexible supporting structure, the anchoring frame structure is widely adopted to support multistage slopes in high earthquake-intensity area for its effectiveness and practicality. The previous study indicates that the anchor of anchoring frame structure is the most likely to be damaged during earthquakes. It is crucial to determine the pull-out capacity of anchor against seismic force for the seismic design of anchoring frame structure. In this study, an analytical model of a three-stage slope supported by anchoring frame structure is established, and the upper bound method of limit analysis is applied to deduce the seismic anchor force of anchoring frame structure. The pull-out capacity of anchor against seismic force of anchoring frame structure at each stage is obtained by computer programming. The proposed method is proved to be reasonable and effective compared with the existing published solution. Besides, the influence of main parameters on the pull-out capacity of anchor against seismic force is analyzed to provide some recommendations for the seismic design of anchoring frame structure.

Keywords: upper bound limit analysis; seismic anchor force; anchoring frame structure; three-stage slope

1. Introduction

The anchor or bolt technology is commonly used to develop a self-anchor structure to control or stabilize the soil slope or rock mass. The anchor or bolt is generally anchored in rock mass to provide sufficient anchor force for self-anchor structure, and the anchor force in self-anchor structure is a key issue that influences the potential failure mechanism of anchoring structure. Consequently, the anchor force as well as its distribution in anchoring structure is concerned by many scholars (Bi *et al.* 2019, Blanco-Fernandez *et al.* 2011, Evirgen *et al.* 2019, Xie *et al.* 2018, Yan and Liang 2019, Zhu *et al.* 2005).

An anchoring frame structure, a kind of self-anchor structure, is widely adopted to stabilize different kinds of slope in engineering practice (Lin *et al.* 2017a, 2020a, 2020b, Shi *et al.* 2019). As a flexible supporting structure, the anchoring frame structure is quite applicable for supporting high slope with multiple stages, which well overcomes the shortcoming of limited height for traditional retaining structure. A photograph of anchoring frame structure that supports a multistage slope in Yun-Gui railway, China is shown in Fig. 1. However, the theory for the seismic analysis of anchoring frame structure is far behind the engineering practice, and the seismic design for slope and retaining or supporting structure is mainly conducted based on a pseudo-static method as well as an empirical method (Lee *et al.* 2019, Motlagh *et al.* 2018, Huang and Chen 2004, Iskander *et al.* 2013, Steedman and Zeng 1990). In pseudo-static method, the earthquake loading is simplified as horizontal or vertical inertial force. The pseudo-static method is available and applicable to some extent, and it is subsequently adopted in the specification of some industrial seismic codes in many countries (Baker *et al.* 2006, Biondi *et al.* 2014, Gursoy and Durmus 2009, Karray *et al.* 2018). In order to improve the pseudo-static method and make it more effective, many scholars analyze the real seismic response of slope and retaining or supporting structure by means of model test and numerical simulation (Anastasopoulos *et al.* 2010, Ling *et al.* 2009, Yazdandoust 2017, 2019b, Zhao *et al.* 2014). Stamatopoulos *et al.* (2007, 2009) applied centrifuge model test and numerical dynamic analysis to illustrate the acceleration amplification near the edge of cliff-type topographies, and the ability to mitigate the topographic effect by anchors and piles was investigated by parametric

*Corresponding author, Associate Professor, Ph.D.
E-mail: linyuliang11@csu.edu.cn, linyuliang11@163.com
[a]Ph.D. Candidate
E-mail: luli050@163.com
[b]Postgraduate
E-mail: 870833101@qq.com
[c]Professor, Senior Engineer
E-mail: 32697916@qq.com
[d]Professor, Senior Engineer
E-mail: 54127636@qq.com
[e]Professor, Senior Engineer
E-mail: 403295922@qq.com
[f]Professor
E-mail: yangguolin6301@163.com

ISSN: 2005-307X (Print), 2092-6219 (Online)

Fig. 1 An anchoring frame structure supporting a multistage slope in Yun-Gui railway, China

analysis. Lin *et al.* (2017b, 2018, 2020c) obtained the distribution of acceleration amplification and the anchor force distribution of anchoring frame beam combined with a gravity wall or a sheet-pile wall by shaking table test and numerical simulation. Zamiran and Osouli (2018) investigated the seismic motion response of a cantilever retaining wall filled by cohesive and cohesionless soil by using finite difference method, and the results were compared to analytical and empirical correlations. Additionally, some scholars also combine the pseudo-static method with the limit equilibrium method (Greco 2014, Nouri *et al.* 2008), the energy-based limit analysis method (Aminpoor and Ghanbari 2014, Aminpour *et al.* 2017, Ranjbar *et al.* 2019), the strength reduction method (Nian *et al.* 2016, Cheng *et al.* 2014), and the Newmark method (Du and Wang 2016, Takaji 2019) to evaluate the seismic stability of slope and retaining or supporting structure, which extends the application of pseudo-static method in seismic analysis.

The mechanism of the anchoring frame structure is much different from that of traditional rigid retaining structure. The frame structure is covering on the soil slope, and it is tightly linked to the rock mass by a series of anchor. When the soil slope is divided into several stages, it would be more complicated to deduce a theoretical formula for the seismic analysis of anchoring frame structure. The previous studies of authors indicate that the anchors in anchoring frame structure are most likely to be damaged subjected to earthquake loading (Lin *et al.* 2017a, b, 2018, 2020a, b). Consequently, it is a key issue to determine the pull-out capacity of anchor against seismic force for the seismic design of anchoring frame structure. With an aim to develop an effective theoretical method for the seismic analysis of anchoring frame structure, the upper bound theorem of limit analysis is adopted to deduce the formula for the seismic anchor force of anchoring frame structure that supports a three-stage slope. The pull-out capacity of anchor against seismic force at each stage is obtained by computer programming with a help of MATLAB platform. Meanwhile, the influence of main parameters on the pull-out capacity of anchor against seismic force is analyzed to provide some recommendations for the seismic design of anchoring frame structure that supports a three-stage slope.

2. Analytical model

To ensure the analytical derivation of seismic anchor force of anchoring frame structure that supports a three-stage slope successful, some basic assumptions are adopted as follows within the framework of upper bound theorem of limit analysis: (1) The analytical model is regarded as a plane-strain problem; (2) The slope soil and rock mass are rigid plastic materials that obey the Mohr-Coulomb criterion and the associated flow rule; (3) The influence of seismic loading on the strength parameters of soil, rock and frame structure is neglected. (4) The horizontal and vertical seismic loading are simplified as inertial forces based on pseudo-static method; (5) The self-weight of frame structure and anchor is small and negligible.

Since the propagation velocity of pressure wave is much faster than that of shear wave in earthquakes, it is not likely that the horizontal acceleration and the vertical acceleration will both reach the peak values at the same time. Consequently, the vertical seismic coefficient (k_v) is determined by making a reduction on horizontal seismic coefficient (k_h), which is expressed as $k_v=\alpha k_h$. And α is commonly determined within a range of 1/3~2/3. The results will critically depend on the values of the horizontal and vertical seismic coefficients. However, there is no specified criterion for the selection of these coefficients. Consequently, the determination of the seismic coefficients has been concerned by many scholars (Bray and Travasarou 2009, Lee *et al*. 2017, Yazdandoust 2019a). In this study, the horizontal and the vertical seismic coefficients are briefly determined based on the degree of seismic intensity according to the seismic design code. For example, the peak values of the horizontal seismic acceleration are set as 0.1 g, 0.3 g, 0.4 g, and 0.6 g that correspond to the seismic intensities of 7°, 8°, 9° and >9°, respectively based on the "Code for Seismic Design of Railway Engineering" of China (GB50111-2006).

An analytical model on the anchoring frame beam that supports a three-stage slope is established based on the upper bound theorem of limit analysis, as shown in Fig. 2. There are two platforms among these three stages of soil slope, and the platform width is represented by d_1 and d_2 respectively. The sliding failure surface is assumed as a logarithmic spiral line that goes through the Point A. The polar coordinate is adopted to simplify the mathematical equation. The length and the rotation angle of Line OA are R_h and θ_h, and they are R_0 and θ_0 for Line OB. The constraint conditions for θ_0 and θ_h are $0<\theta_0<180°$ and $\theta_0<\theta_h<180°$, respectively. The height coefficient (α) is defined as a ratio of the slope height at each stage (i.e., H_{I}, H_{II}, and H_{III}) to the total height of soil slope (H), and the height coefficient of these three stages of soil slope are symbolized by α_1, α_2, and α_3 respectively. The slope angle of these three stages are β_1, β_2, and β_3 respectively. The anchor is inclined at ξ (i.e., anchorage angle) with the horizontal surface. z_i refers to the vertical distance from the intersection point between the anchor and the potential failure surface to the top surface of soil slope (i.e., Line BC). The logarithmic spiral surface AB is a kind of velocity discontinuity based on the associated flow rule. When the soil is in a plastic flow state, the dilatation angle between the velocity and the tangent line at any point of potential failure surface is regarded to be equal to the internal friction angle of sliding soil φ. The rigid potential sliding body $ABCD_1D_2E_1E_2A$ tends to rotate around the Point O at an

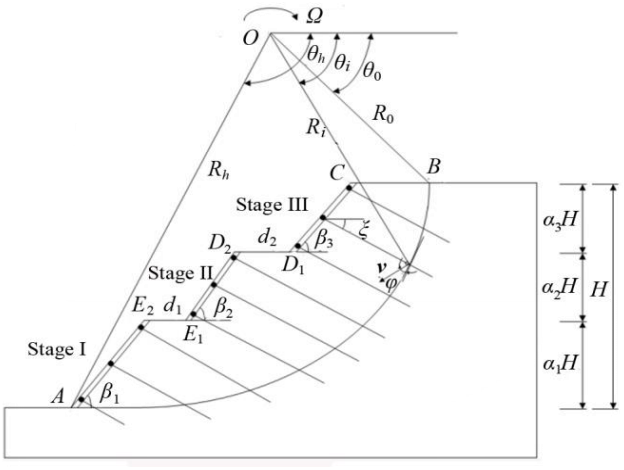

Fig. 2 Failure mechanism of anchoring frame structure supporting a three-stage slope

angular velocity of Ω.

The logarithmic spiral line *AB* can be expressed as:

$$R(\theta) = R_0 \cdot e^{(\theta-\theta_0)\tan\varphi} \tag{1}$$

in which, $R(\theta)$ refers to a polar radius in polar coordinate, and θ is the polar angle for logarithmic spiral line *AB*.

According to the geometric relationship, H/R_0, L/R_0 can be expressed as the functions of θ_0 and θ_h:

$$H / R_0 = \sin\theta_h \cdot e^{(\theta_h-\theta_0)\tan\varphi} - \sin\theta_0 \tag{2}$$

$$\begin{aligned} L / R_0 &= \cos\theta_0 - \cos\theta_h \cdot e^{(\theta_h-\theta_0)\tan\varphi} \\ &\quad -(\alpha_1 \cot\beta_1 + \alpha_2 \cot\beta_2' + \alpha_3 \cot\beta_3') \cdot H / R_0 \end{aligned} \tag{3}$$

in which, L refers to the length of BC; β_2' denotes the angle between Line E_2D_2 and Line E_2E_1, and β_3' is the angle between Line D_2C and Line D_2D_1. And they can be determined by the equations of $\cot\beta_2' = \cot\beta_2 + d_1/\alpha_2 H$ and $\cot\beta_3' = \cot\beta_3 + d_2/\alpha_3 H$.

3. Energy calculation

According to the upper bound theorem of plastic limit analysis, the rigid-plastic soil slope tends to fail in the kinematically admissible velocity field when the external force power is equal to the internal energy dissipation. Consequently, it is crucial to determine the internal energy dissipation and the external force power.

3.1 Internal energy dissipation

Based on the analytical model of the failure mechanism of anchoring frame structure (see Fig. 2), the internal energy dissipation (P_{int}) mainly occurs along the velocity discontinuity surface (i.e., potential failure surface *AB*), which consists of the energy dissipation related to the shear strength of soil (P_c) and the force power caused by a series of anchor (P_t). Based on Mohr-Coulomb criterion, the energy dissipation of P_c can be determined by integrating the vector product of the soil cohesion (c) and the discontinuity velocity of the microelement over the entire potential sliding surface *AB*, which can be expressed as following:

$$\begin{aligned} P_c &= \int_{\theta_0}^{\theta_h} c \cdot V \cos\varphi \cdot \frac{R \cdot \mathrm{d}\theta}{\cos\varphi} \\ &= cR_0^2\Omega \cdot \frac{e^{2(\theta_h-\theta_0)\tan\varphi} - 1}{2\tan\varphi} \end{aligned} \tag{4}$$

in which, "V" refers to the the velocity at any point of the discontinuity surface *AB*.

The anchor force is taken to balance the earth pressure on frame structure. According to the geometrical relationship of the anchorage angle ξ and the rotation angle θ_i along the potential failure surface *AB*, the total force power caused by a series of anchor (P_t) can be expressed as following:

$$P_t = \sum_{i=1}^{n} T_i \cdot R_0 e^{(\theta_i-\theta_0)\tan\varphi} \cdot \Omega \cdot \sin|\theta_i - \xi| \tag{5}$$

in which, T_i is the seismic anchor force of the i-th anchor of anchoring frame structure..

For a certain anchoring frame structure, the anchorage angle ξ is known. To make the analytical derivation more efficient, the term of $R_0 e^{(\theta_i-\theta_0)\tan\varphi} \cdot \sin|\theta_i - \xi|$ in Eq. (5) is represented by m_{i1}, m_{i2}, and m_{i3} for Stages I, II, and III of anchoring frame structure, which can be deduced as following:

$$\begin{aligned} m_{i3} &= R_0 e^{(\theta_i-\theta_0)\tan\varphi} \cdot \sin|\theta_i - \xi| \\ &= \left|\sin\xi\left[z_i \cot\beta_3 - R_h\cos\theta_h - (d_1+d_2) - \sum_{m=1}^{3}\alpha_m H\cot\beta_m\right] + \cos\xi(z_i + R_0\sin\theta_0)\right| \\ &= \left|\sin\xi\left[z_i\cot\beta_3 - (H/R_0)^{-1} H\cdot e^{(\theta_h-\theta_0)\tan\varphi}\cos\theta_h - (d_1+d_2) - \sum_{m=1}^{3}\alpha_m H\cot\beta_m\right]\right. \\ &\quad \left. + \cos\xi\left(z_i + (H/R_0)^{-1} H\sin\theta_0\right)\right| \end{aligned} \tag{6}$$

$$\begin{aligned} m_{i2} &= R_0 e^{(\theta_i-\theta_0)\tan\varphi} \cdot \sin|\theta_i - \xi| \\ &= \left|\sin\xi\left[(z_i - \alpha_3 H)\cot\beta_2 - R_h\cos\theta_h - d_1 - \sum_{m=1}^{2}\alpha_m H\cot\beta_m\right] + \cos\xi(z_i + R_0\sin\theta_0)\right| \\ &= \left|\sin\xi\left[(z_i - \alpha_3 H)\cot\beta_2 - (H/R_0)^{-1} H\cdot e^{(\theta_h-\theta_0)\tan\varphi}\cos\theta_h - d_1 - \sum_{m=1}^{2}\alpha_m H\cot\beta_m\right]\right. \\ &\quad \left. + \cos\xi\left(z_i + (H/R_0)^{-1} H\sin\theta_0\right)\right| \end{aligned} \tag{7}$$

$$\begin{aligned} m_{i1} &= R_0 e^{(\theta_i-\theta_0)\tan\varphi} \cdot \sin|\theta_i - \xi| \\ &= \left|\sin\xi\left[(z_i - \alpha_2 H - \alpha_3 H)\cot\beta_1 - R_h\cos\theta_h - \alpha_1 H\cot\beta_1\right] + \cos\xi(z_i + R_0\sin\theta_0)\right| \\ &= \left|\sin\xi\left[(z_i - \alpha_2 H - \alpha_3 H)\cot\beta_1 - (H/R_0)^{-1} H\cdot e^{(\theta_h-\theta_0)\tan\varphi}\cos\theta_h - \alpha_1 H\cot\beta_1\right]\right. \\ &\quad \left. + \cos\xi\left(z_i + (H/R_0)^{-1} H\sin\theta_0\right)\right| \end{aligned} \tag{8}$$

3.2 External force power

Based on the potential failure mechanism of anchoring frame structure, the external force power is mainly induced by the gravity of soil mass and the seismic loading. In other word, the external force power P_{ext} is composed of the gravity-induced power of soil mass P_g, the power induced by the horizontal seismic loading P_h, and the power induced by the vertical seismic loading P_v.

To make the derivation of the gravity-induced power

more convenient, the power caused by the gravity of rigid soil body $ABCD_1D_2E_1E_2A$ (P_g) can be regarded as a superposition of the powers induced by the gravity of Areas OAB, OBC, OCD_1, OD_1D_2, OD_2E_1, OE_1E_2, and OE_2A (see Fig. 2), which are represented by P_0, P_1, P_2, P_3, P_4, P_5, and P_6, respectively. Subsequently, the equation for P_g is expressed as:

$$P_g = P_0 - P_1 - P_2 - P_3 - P_4 - P_5 - P_6 \tag{9}$$

The power caused by the gravity of Area OAB can be integrated along the potential sliding surface AB in polar coordinate. The gravity-induced power of the other areas (i.e., Areas OBC, OCD_1, OD_1D_2, OD_2E_1, OE_1E_2, and OE_2A) can be determined as a vector product of the gravity of soil and the vertical velocity at the barycenter. Subsequently, the expressions for P_0~P_6 can be expressed in an uniform form as follows:

$$P_n = \gamma R_0^3 \Omega \cdot f_n \quad (n=0, 1, 2, ..., 6) \tag{10}$$

in which, f_n (n=0,1,2,...,6) are all functions of θ_0 and θ_h, which are presented in "Appendix 1".

Thereafter, the power caused by the gravity of rigid soil body $ABCD_1D_2E_1E_2A$ (P_g) can be determined as:

$$P_g = \gamma R_0^3 \Omega \cdot (f_0 - \sum_{n=1}^{6} f_n) \tag{11}$$

The power caused by horizontal seismic loading (P_h) can also be regarded as a superposition of the powers of Areas OAB, OBC, OCD_1, OD_1D_2, OD_2E_1, OE_1E_2, and OE_2A. Subsequently, the power caused by horizontal seismic loading (P_h) can be expressed as:

$$P_h = k_h \cdot \gamma R_0^3 \Omega \cdot (g_0 - \sum_{n=1}^{6} g_n) \tag{12}$$

in which, k_h refers to the horizontal seismic coefficient; g_0~g_6 are all functions of θ_0 and θ_h, which are presented in "Appendix 2".

Similarly, the power caused by vertical seismic loading P_v can be obtained as following:

$$P_v = -k_v \cdot \gamma R_0^3 \Omega \cdot (f_0 - \sum_{n=1}^{6} f_n) \tag{13}$$

in which, k_v refers to the vertical seismic coefficient.

Thereafter, the external power P_{ext} can be obtained as:

$$P_{\text{ext}} = \gamma R_0^3 \Omega \left[(1-k_v)F_0 + k_h G_0\right] \tag{14}$$

where, $F_0 = f_0 - \sum_{n=1}^{6} f_n$, and $G_0 = g_0 - \sum_{n=1}^{6} g_n$.

4. Seismic anchor force

4.1 Equation for seismic anchor force

In engineering practice, an inverse measure is commonly applied for the construction of anchoring frame structure that supports a multistage slope. The inverse measure takes the construction sequence from the top to the bottom, which means that the anchoring frame structure at the top stage of soil slope is firstly constructed, and the excavation on the soil mass is carried out downwards. According to the construction process of inverse measure, the seismic anchor force at the top stage (i.e., Stage III) of soil slope can be firstly determined based on an one-stage slope model. Subsequently, the seismic anchor forces for the next two stages (i.e., Stages II and I) of soil slope can be obtained based on a two-stage or a three-stage soil slope model.

Based on the upper bound theorem of plastic limit analysis, the soil mass will be in a plastic limit equilibrium state when the internal energy dissipation is equal to the external force power, which can be expressed as following:

$$P_c + P_t = P_g + P_h + P_v \tag{15}$$

By substituting Eqs. (4)-(5) and Eqs. (11)-(13) into Eq. (15), the seismic anchor force of anchoring frame structure supporting a three-stage soil slope can be established while taking the horizontal spacing of anchor (S_x) into consideration:

$$\begin{aligned} \sum_{i=1}^{n} T_i \cdot R_0 e^{(\theta_i-\theta_0)\tan\varphi} \cdot \sin\left|\theta_i - \xi\right| \\ = S_x \gamma H^3 \cdot (H/R_0)^{-3}\left[(1-k_v)F_0 + k_h G_0\right] \\ - S_x c H^2 \cdot (H/R_0)^{-2} \cdot \frac{e^{2(\theta_h-\theta_0)\tan\varphi}-1}{2\tan\varphi} \end{aligned} \tag{16}$$

in which, T_i denotes the seismic anchor force of anchoring frame structure; n refers to total number of anchor; γ is the unit weight of soil mass; S_x means the horizontal spacing of anchor.

4.2 Anchor force at different stages

The number of anchors at Stages I, II, and III of soil slope is represented by n_{I}, n_{II}, and n_{III} respectively. As for the Stage III, the following condition can be obtained based on the analytical model of anchoring frame structure: $\alpha_1=\alpha_2=0$, $d_1=d_2=0$, $\beta_1=\beta_2=0$, $H_{\text{III}}=\alpha_3 H$, $f_3=f_4=f_5=f_6=0$, and $g_3=g_4=g_5=g_6=0$. The formula for the seismic anchor force at Stage III (T_{III}) can be established based on a one-stage slope model as following:

$$T_{\text{III}} = \frac{\begin{aligned} &S_x \gamma H_{\text{III}}^3 \cdot (H_{\text{III}}/R_0)^{-3}\left[(1-k_v)F_0 + k_h G_0\right] \\ &-S_x c H_{\text{III}}^2 \cdot (H_{\text{III}}/R_0)^{-2} \cdot \frac{e^{2(\theta_h-\theta_0)\tan\varphi}-1}{2\tan\varphi} \end{aligned}}{\sum_{i=1}^{n_{\text{III}}} m_{i3}} \tag{17}$$

Based on the mechanism of anchoring frame structure, the potential failure surface AB is determined by θ_0 and θ_h. Meanwhile, different values of θ_0 and θ_h would induce different values of seismic anchor force of anchoring frame structure. To determine the pull-out capacity of anchor against seismic force of anchoring frame beam for each stage of soil slope, the equations of $\partial T_{\text{III}}/\partial\theta_0 = 0$ and $\partial T_{\text{III}}/\partial\theta_h = 0$ can be applied. In which, θ_0 and θ_h are subjected to the constraint condition of $0<\theta_0<180°$ and

Table 1 Comparison between the present method and solution of Yan *et al.* (2019)

Height of slope (m)	Slope angle (º)	Anchor angle (º)	Cohesion (kPa)	Friction angle (º)	Horizontal seismic coefficient	Vertical seismic coefficient	Factor of Safety	Seismic anchor force (kN)		Deviation (%)
								Yan *et al.* (2019)	Proposed method	
10	60	20	12	25	0.2	0.1	1.245	100.0	108.4	8.40
10	60	20	12	25	0.2	0.1	1.202	90.0	93.9	4.33
10	60	20	12	25	0.2	0.1	1.146	80.0	81.8	2.25

$\theta_0<\theta_h<180°$. Based on a global optimization algorithm, the values of θ_0 and θ_h can be determined by computer programming based on the Matlab platform. Subsequently, the pull-out capacity of anchor against seismic force at Stage III of soil slope can be obtained.

As for the Stage II, based on the condition of $\alpha_1=0$, $d_1=0$, $\beta_1=0$, $H_{II}=(\alpha_2+\alpha_3)H$, $f_5=f_6=0$, and $g_5=g_6=0$, the formula for the seismic anchor force at Stage II (T_{II}) can be established while considering the effect of anchor force at the Stage III (T_{III}), which is expressed as following:

$$T_{II}=\frac{\begin{array}{l}S_x\gamma H_{II}^3\cdot(H_{II}/R_0)^{-3}\left[(1-k_v)F_0+k_hG_0\right]\\-S_xcH_{II}^2\cdot(H_{II}/R_0)^{-2}\cdot\dfrac{e^{2(\theta_h-\theta_0)\tan\varphi}-1}{2\tan\varphi}\\-T_{III}\sum\limits_{i=1}^{n_{III}}m_{i3}\end{array}}{\sum\limits_{i=n_{III}+1}^{n_{III}+n_{II}}m_{i2}} \tag{18}$$

The pull-out capacity of anchor against seismic force at Stage II (T_{II}) can also be obtained by supposing $\partial T_{II}/\partial\theta_0=0$ and $\partial T_{II}/\partial\theta_h=0$.

As for the Stage I, it is seen that $H_I=(\alpha_1+\alpha_2+\alpha_3)H=H$. The formula for the seismic anchor force at Stage I (T_I) can be established while considering the effect of anchor force of Stage III (T_{III}) as well as that of Stage II (T_{II}), which is expressed as following:

$$T_I=\frac{\begin{array}{l}S_x\gamma H_I^3\cdot(H_I/R_0)^{-3}\left[(1-k_v)F_0+k_hG_0\right]\\-S_xcH_I^2\cdot(H_I/R_0)^{-2}\cdot\dfrac{e^{2(\theta_h-\theta_0)\tan\varphi}-1}{2\tan\varphi}\\-T_{III}\sum\limits_{i=1}^{n_{III}}m_{i1}-T_{II}\sum\limits_{i=n_{III}+1}^{n_{III}+n_{II}}m_{i1}\end{array}}{\sum\limits_{i=n_{II}+n_{III}+1}^{n_I+n_{II}+n_{III}}m_{i1}} \tag{19}$$

Likewise, the pull-out capacity of anchor against seismic force at Stage I (T_I) can be determined by supposing $\partial T_I/\partial\theta_0=0$, $\partial T_I/\partial\theta_h=0$.

5. Comparison

Most of the existing literature are concentrated on a one-stage soil slope supported by anchoring structure. This study proposed an analytical solution for seismic anchor force of anchoring frame structure that supports a three-stage soil slope. The analytical solution of this study is still workable for the case of one-stage soil slope. Consequently, a typical comparison is made between the analytical solution of this study and the result proposed by Yan *et al.* (2019). Yan *et al.* (2019) applied a limit analysis and a pseudo-dynamic method to determine the safety of factor (F_s) of a one-stage soil slope reinforced by anchor cables. A special case is considered (namely Condition A in literature) in which the dynamic change of axial force of anchor under seismic excitation are neglected. The parameters for theoretical analysis in this case are listed below: H=10 m, β=60°, c=12 kPa, φ=25°, γ=18 kN/m^3, ξ=20°, S_x=3 m, k_h=0.2 and k_v=0.1. Based on the research of Yan *et al.* (2019), the values for the factor of safety (F_s) are 1.245, 1.202 and 1.146 when the axial forces of anchor are 100.0 kN, 90.0 kN and 80.0 kN, respectively.

This study focuses on the solution for the pull-out capacity of anchor against seismic force of anchoring frame structure. The pull-out capacity of anchor against seismic force is regarded as the one that makes the anchoring frame structure meet the minimum requirement for stability. Thus, the factor of safety of anchoring frame structure should be 1.0 in this situation. To make the comparison successful and reasonable, the strength parameters of soil are reduced by $c'=c/F_s$ and $\tan\varphi'=\tan\varphi/F_s$ in this study based on the definition of the factor of safety. Subsequently, the results determined by proposed method can be reasonably compared with that determined by Yan *et al.* (2019), which are shown in Table1. The results show that the proposed method provides a good estimation on the seismic anchor force of anchoring frame structure with the maximum deviation being less than 8.40%, which is totally acceptable for seismic design and engineering practice.

6. Influence of parameters

For some recommendations related to the seismic design of anchoring frame structure, the influence of seven main parameters on the pull-out capacity of anchor against seismic force of anchoring frame structure is analyzed, including the horizontal and vertical seismic coefficients k_h and k_v, the slope angle at each stage β_i, the anchorage angle ξ, the horizontal spacing of anchor S_x, the strength reduction coefficient (factor of safety) F_s, and the platform width d_i. The cohesion and the internal friction angle of soil are fixed as c=19.8 kPa and φ=35.0°. The spacing of adjective anchors along the slope surface is about 3 m. The total height of soil slope is H=18 m, and the values of soil slope height for each stage are all 6 m, which indicates that $\alpha_1=\alpha_2=\alpha_3=1/3$. The concept of orthogonal design is adopted to evaluate the vulnerability of seismic anchor force at each stage to different parameters. Without a consideration on

Table 2 Four levels for seven main parameters based on the concept of orthogonal design

Level	k_h	k_v	F_s	S_x (m)	d_i (m)	ξ (º)	β_i (º)
I	0.1	$1/3k_h$	1.00	2.0	I	15	I
II	0.3	$1/2k_h$	1.10	2.5	II	20	II
III	0.4	$2/3k_h$	1.25	3.0	III	30	III
IV	0.6	k_h	1.50	4.0	IV	40	IV

Table 3 The pull-out capacity of anchor against seismic force at different stages based on orthogonal design

No	k_h	k_v	F_s	S_x (m)	d_i (m)	ξ (º)	β_i (º)	T_{I} (kN)	T_{II} (kN)	T_{III} (kN)
1	0.1	$1/3k_h$	1.00	2.0	I	15	II	55.73	47.58	14.68
2	0.1	$1/3k_h$	1.10	3.0	II	20	III	517.64	220.62	53.80
3	0.1	$1/3k_h$	1.25	2.5	III	40	IV	129.18	371.94	96.20
4	0.1	$1/3k_h$	1.50	4.0	IV	30	I	427.38	78.02	71.43
5	0.1	$1/2k_h$	1.00	2.0	II	20	III	233.64	121.95	54.67
6	0.1	$1/2k_h$	1.10	3.0	III	30	IV	79.47	46.37	12.44
7	0.1	$1/2k_h$	1.25	2.5	IV	40	I	264.17	189.97	102.96
8	0.1	$1/2k_h$	1.50	4.0	I	15	II	57.54	35.93	13.38
9	0.1	$2/3k_h$	1.00	3.0	III	30	I	73.21	31.22	13.17
10	0.1	$2/3k_h$	1.10	4.0	IV	40	III	686.61	427.56	163.91
11	0.1	$2/3k_h$	1.25	2.0	I	15	IV	1054.59	548.78	156.30
12	0.1	$2/3k_h$	1.50	2.5	II	20	II	628.35	203.66	148.72
13	0.1	k_h	1.00	4.0	I	15	I	171.29	159.76	57.13
14	0.1	k_h	1.10	3.0	III	30	III	226.22	121.95	54.67
15	0.1	k_h	1.25	4.0	IV	40	II	558.14	258.48	87.93
16	0.1	k_h	1.50	2.5	II	20	IV	852.01	527.49	196.98
17	0.3	$1/3k_h$	1.00	2.5	I	15	III	173.62	127.08	34.42
18	0.3	$1/3k_h$	1.10	3.0	III	30	II	1190.62	725.74	429.22
19	0.3	$1/3k_h$	1.25	4.0	II	20	IV	919.64	726.56	498.54
20	0.3	$1/3k_h$	1.50	2.0	IV	40	I	402.08	265.69	57.69
21	0.3	$1/2k_h$	1.00	3.0	III	30	III	242.36	110.86	27.40
22	0.3	$1/2k_h$	1.10	2.0	II	20	I	462.89	326.51	132.41
23	0.3	$1/2k_h$	1.25	4.0	IV	40	II	132.07	91.52	43.22
24	0.3	$1/2k_h$	1.50	2.5	I	15	IV	680.36	135.79	45.62
25	0.3	$2/3k_h$	1.00	2.5	III	30	III	585.27	451.49	123.22
26	0.3	$2/3k_h$	1.10	4.0	I	15	II	473.30	389.97	102.96
27	0.3	$2/3k_h$	1.25	2.0	II	30	IV	50.28	46.62	39.21
28	0.3	$2/3k_h$	1.50	3.0	IV	20	I	814.82	449.26	441.59
29	0.3	k_h	1.00	2.5	III	40	I	306.67	280.34	125.05
30	0.3	k_h	1.10	3.0	II	20	II	806.63	465.91	55.33
31	0.3	k_h	1.25	4.0	IV	40	I	1161.64	280.84	417.83
32	0.3	k_h	1.50	2.0	I	15	IV	545.36	180.96	159.01
33	0.4	$1/3k_h$	1.00	2.0	I	15	I	1089.41	1509.91	561.88
34	0.4	$1/3k_h$	1.10	2.5	III	20	III	98.68	97.20	43.21
35	0.4	$1/3k_h$	1.25	3.0	IV	30	I	939.62	252.03	209.63
36	0.4	$1/3k_h$	1.50	2.0	II	40	II	280.38	286.61	149.19
37	0.4	$1/2k_h$	1.00	2.5	I	15	IV	1088.20	449.74	371.12

Table 3 Continued

No	k_h	k_v	F_s	S_x (m)	d_i (m)	ξ (°)	β_i (°)	T_{I} (kN)	T_{II} (kN)	T_{III} (kN)
38	0.4	1/2k_h	1.10	3.0	II	30	II	471.18	405.62	129.56
39	0.4	1/2k_h	1.25	4.0	III	40	III	195.04	158.89	39.16
40	0.4	1/2k_h	1.50	2.0	IV	20	I	132.53	119.19	49.60
41	0.4	2/3k_h	1.00	3.0	I	40	I	946.60	722.34	254.82
42	0.4	2/3k_h	1.10	2.5	III	20	IV	355.40	88.83	253.71
43	0.4	2/3k_h	1.25	2.0	IV	30	III	947.16	533.03	143.98
44	0.4	2/3k_h	1.50	4.0	II	15	II	484.26	243.08	184.24
45	0.4	k_h	1.00	2.0	IV	15	II	1284.91	1527.28	683.88
46	0.4	k_h	1.10	4.0	II	40	IV	857.19	792.82	608.73
47	0.4	k_h	1.25	3.0	III	30	III	643.97	234.56	241.66
48	0.4	k_h	1.50	2.5	I	20	I	1287.96	584.30	572.74
49	0.6	1/3k_h	1.00	2.0	I	20	II	1496.15	858.38	641.80
50	0.6	1/3k_h	1.10	4.0	IV	40	IV	302.22	136.51	79.97
51	0.6	1/3k_h	1.25	3.0	III	30	I	1679.21	2092.88	1054.56
52	0.6	1/3k_h	1.50	2.5	II	15	III	230.58	177.41	65.71
53	0.6	1/2k_h	1.00	2.0	II	20	IV	356.62	314.82	60.80
54	0.6	1/2k_h	1.10	4.0	IV	40	II	1485.07	964.12	885.43
55	0.6	1/2k_h	1.25	2.5	III	15	III	238.26	135.90	70.39
56	0.6	1/2k_h	1.50	3.0	I	30	I	532.32	430.76	184.24
57	0.6	2/3k_h	1.00	4.0	II	15	I	1381.69	922.06	538.01
58	0.6	2/3k_h	1.10	2.5	IV	30	II	1179.94	699.71	237.67
59	0.6	2/3k_h	1.25	3.0	I	40	III	581.48	345.55	241.66
60	0.6	2/3k_h	1.50	2.0	III	20	IV	1767.76	1056.99	829.05
61	0.6	k_h	1.00	2.5	IV	40	I	1295.24	520.23	384.54
62	0.6	k_h	1.10	4.0	II	20	III	435.39	399.14	212.20
63	0.6	k_h	1.25	2.0	III	30	IV	55.73	47.58	14.68
64	0.6	k_h	1.50	3.0	I	15	II	517.64	220.62	53.80

the correlations among parameters, the above mentioned seven parameters are designed as four levels based on experience of engineering practice, as listed in Table 2. In which, the levels for the platform width d_i are as following: d_1=2.5 m and d_2=2.0 m for Level I; d_1=3.0 m and d_2=2.5 m for Level II; d_1=4.0 m and d_2=3.0 m for Level III; d_1=5.0 m and d_2=4.0 m for Level IV. The levels for the slope angle at each stage β_i are as following: β_1=60°, β_2=45° and β_3=30° for Level I; β_1=60°, β_2=60° and β_3=60° for Level II; β_1=70°, β_2=60° and β_3=45° for Level III; β_1=80°, β_2=70° and β_3=60° for Level IV. The different levels essentially reflect the range that the parameters changes within in this analysis. Meanwhile, it is noted that the analysis results may be different if the parameter level changes.

Based on the orthogonal design, 64 sets of data for the pull-out capacity of anchor against seismic force at different stages are obtained, as shown in Table 3. Since the above mentioned parameters are designed as 4 levels, there are 16 sets of data for every parameter at each level. An average value of seismic anchor force is calculated based on 16 sets of data for every parameter at each level, as shown in Table 4. In which, the maximum difference is determined by using the maximum one minus the minimum one, which reflects the influencing sensitivity of parameter on the pull-out capacity of anchor against seismic force at different stages. For example, as the level of horizontal seismic coefficient k_h changes from I to IV (k_h increases from 0.1 to 0.6), the pull-out capacity of anchor against seismic force at Stage I (T_{I}) increases from 347.43 kN to 1707.74 kN with the maximum difference of 1360.31 kN. Compared with the other parameters, the maximum difference for T_{I} related to k_h is the largest. Meanwhile, the values of the maximum difference related to k_h for the pull-out capacity of anchor against seismic force at Stages II and III (T_{II} and T_{III}) are 392.22 kN and 314.93 kN respectively, which are also larger than the maximum difference induced by other parameters. Consequently, it is concluded that the pull-out capacity of anchor against seismic force is the most sensitive to the horizontal seismic coefficient k_h. By comparing the maximum difference of the pull-out capacity of anchor against seismic force among the different parameters, the rank of influencing sensitivity of above mentioned parameters can be obtained. As for the seismic

Table 4 The maximum difference analysis of seven main parameters based on the results of orthogonal design

Parameters	T_i (kN)	Level				Maximum difference
		I	II	III	IV	
k_h	T_{I}	347.43	578.39	627.06	1707.74	1360.31
	T_{II}	224.87	337.61	465.77	617.08	392.22
	T_{III}	78.84	173.17	243.60	393.78	314.93
k_v	T_{I}	620.76	615.73	650.67	687.87	72.14
	T_{II}	498.38	452.37	447.51	412.64	85.74
	T_{III}	253.87	238.90	242.01	245.39	14.97
F_s	T_{I}	673.79	601.78	596.89	602.58	76.90
	T_{II}	409.69	394.29	394.70	312.24	97.46
	T_{III}	246.66	215.95	216.12	201.44	45.23
S_x	T_{I}	623.61	568.75	611.72	641.23	72.48
	T_{II}	425.59	298.25	409.97	457.29	159.04
	T_{III}	211.50	172.70	208.27	279.88	107.18
d_i	T_{I}	689.03	623.32	582.94	550.03	139.00
	T_{II}	437.35	432.39	421.32	300.06	137.29
	T_{III}	236.36	224.39	243.92	167.68	68.68
ξ	T_{I}	619.05	651.26	582.75	592.27	68.51
	T_{II}	455.63	372.58	394.28	368.62	87.01
	T_{III}	224.02	236.31	186.67	225.34	49.64
β_i	T_{I}	567.61	581.74	634.87	661.11	93.50
	T_{II}	315.61	395.05	439.66	440.80	125.19
	T_{III}	187.92	171.84	260.41	252.18	80.34

anchor force at Stage I (T_{I}), the sensitivity rank for the above parameters is listed as following: the horizontal seismic coefficient k_h, the platform width d_i, the slope angle of each stage β_i, the strength reduction coefficient F_s, the horizontal spacing of anchor S_x, the vertical seismic coefficients k_v, and the anchorage angle ξ. The sensitivity rank of parameters for the seismic anchor force at Stage II (T_{II}) is the same as that at Stage III (T_{III}), and it is k_h, S_x, d_i, β_i, F_s, ξ, and k_v.

With regard to the engineering design of anchoring frame structure, the geometrical shape of anchoring structure are much related to the horizontal spacing of anchor S_x, the platform width d_i, the anchorage angle ξ, and the slope angle at each stage β_i. According to above results, the pull-out capacity of anchor against seismic force at each stage reaches the least value when the horizontal spacing of anchor S_x is equal to 2.5 m. The pull-out capacity of anchor against seismic force decreases with the increase of the platform width d_i, and it increases as the slope angle of each stage β_i increases. The pull-out capacity of anchor against seismic force at different stages does not show a monotonous tendency asthe anchorage angle ξ increases within a range of 15-40°, and the maximum difference of seismic anchor force related to ξ is not so great. Consequently, to make a reasonable seismic design of anchoring frame structure, it is recommended that the anchor horizontal spacing could be determined at approximately 2.5 m. It is preferable to set the anchorage angle of anchor within a range of 20-40°. Meanwhile, the mutual interaction among different stages should be considered. A larger platform width and a smaller slope angle of each stage will greatly improve the mechanical behavior of anchors. Additionally, since the seismic anchor force is the most sensitive to the horizontal seismic coefficient, the anchor with a large tensile strength is recommended in high earthquake-intensity areas, especially for the anchors at Stage I.

7. Conclusions

Based on the upper bound theorem of plastic limit analysis, the failure mechanism of an anchoring frame structure that supports a three-stage slope is established. The internal energy dissipation and the external force power are obtained, and the formula for seismic anchor force of anchoring frame structure at different stages are deduced. The pull-out capacity of anchor against seismic force at different stages are determined by optimization with a help of computer programming based on MATLAB platform. The proposed method is compared with a previous published solution to verify its rationality.

The concept of orthogonal design is adopted to evaluate the vulnerability of seismic anchor force at each stage to different parameters, including the horizontal and vertical seismic coefficients, the slope angle at each stage, the

anchorage angle, the horizontal spacing of anchor, the strength reduction coefficient of soil, and the platform width. The pull-out capacity of anchor against seismic force of anchoring frame structure is the most sensitive to the horizontal seismic coefficient.

As for the seismic design of anchoring frame structure, it is recommended to set a value of approximately 2.5 m for the anchor horizontal spacing. It is preferable to set the anchorage angle of anchor within a range of 20-40º. A larger platform width and a smaller slope angle at each stage are beneficial to the mechanical behavior of anchors. In high earthquake-intensity areas, the anchor with a large tensile strength is necessary, especially for the anchors at Stage I.

Acknowledgments

The authors sincerely acknowledge the financial support from the National Natural Science Foundation of China (Grant Nos. 51878667, 51678571, 51308551), and the Hunan Provincial Natural Science Foundation of China (Grant No. 2018JJ2517). The first author gratefully acknowledges the financial support from China Scholarship Council (Grant No. 201806375024). The authors also acknowledge the helpful comments on this paper from anonymous reviewers.

References

Aminpoor, M.M. and Ghanbari, A. (2014), "Design charts for yield acceleration and seismic displacement of retaining walls with surcharge through limit analysis", *Struct. Eng. Mech.*, **52**(6), 1225-1256. https://doi.org/10.12989/sem.2014.52.6.1225.

Aminpour, M.M., Maleki, M. and Ghanbari, A. (2017), "Investigation of the effect of surcharge on behavior of soil slopes", *Geomech. Eng.*, **13**(4), 653-669. https://doi.org/10.12989/gae.2017.13.4.653.

Anastasopoulos, I., Georgarakos, T., Georgiannou, V., Drosos, V. and Kourkoulis, R. (2010), "Seismic performance of bar-mat reinforced-soil retaining wall: Shaking table testing versus numerical analysis with modified kinematic hardening constitutive model", *Soil Dyn. Earthq. Eng.*, **30**(10), 1089-1105. https://doi.org/10.1016/j.soildyn.2010.04.020.

Baker, R., Shukha, R., Operstein, V. and Frydman, S. (2006), "Stability charts for pseudo-static slope stability analysis", *Soil Dyn. Earthq. Eng.*, **26**(9), 813-823. https://doi.org/10.1016/j.soildyn.2006.01.023.

Bi, J., Luo, X., Zhang, H. and Shen, H. (2019), "Stability analysis of complex rock slopes reinforced with prestressed anchor cables and anti-shear cavities", *B. Eng. Geol. Environ.*, **78**(3), 2027-2039. http://doi.org/10.1007/s10064-017-1171-8.

Biondi, G., Cascone, E. and Maugeri, M. (2014), "Displacement versus pseudo-static evaluation of the seismic performance of sliding retaining walls", *B. Earthq. Eng.*, **12**(3), 1239-1267. https://doi.org/10.1007/s10518-013-9542-4.

Blanco-Fernandez, E., Castro-Fresno, D., Diaz, J.J.D. and Lopez-Quijada, L. (2011), "Flexible systems anchored to the ground for slope stabilisation: Critical review of existing design methods", *Eng. Geol.*, **122**(3-4), 129-145. https://doi.org/10.1016/j.enggeo.2011.05.014.

Bray, J.D. and Travasarou, T. (2009), "Pseudostatic coeffificient for use in simplifified seismic slope stability evaluation", *J. Geotech. Geoenviron. Eng.*, **135**(9), 1336-1340. http://doi.org/10.1061/(ASCE)GT.1943-5606.0000012.

Cheng, X.S., Dowding, C.H. and Tian, R.R. (2014), "New methods of safety evaluation for rock/soil mass surrounding tunnel under earthquake", *J. Cent. South Univ.*, **21**(7), 2935-2943. https://doi.org/10.1007/s11771-014-2260-5.

Du, W.Q. and Wang, G. (2016), "A one-step Newmark displacement model for probabilistic seismic slope displacement hazard analysis", *Eng. Geol.*, **205**, 12-23. https://doi.org/10.1016/j.enggeo.2016.02.011.

Evirgen, B., Tuncan, A. and Tuncan, M. (2019), "Development of umbrella anchor approach in terms of the requirements of field application", *Geomech. Eng.*, **18**(3), 277-289. https://doi.org/10.12989/gae.2019.18.3.277.

Greco, V.R. (2014), "Analytical solution of seismic pseudo-static active thrust acting on fascia retaining walls", *Soil Dyn. Earthq. Eng.*, **57**, 25-36. https://doi.org/10.1016/j.soildyn.2013.09.022.

Gursoy, S. and Durmus, A. (2009), "Investigation of linear and nonlinear of behaviours of reinforced concrete cantilever retaining walls according to the earthquake loads considering soil-structures interactions", *Struct. Eng. Mech.*, **31**(1), 75-91. https://doi.org/10.12989/sem.2009.31.1.075.

Huang, C.C. and Chen, Y.H. (2004), "Seismic stability of soil retaining walls situated on slope", *J. Geotech. Geoenviron. Eng.*, **130**(1), 45-57. http://doi.org/10.1061/(ASCE)1090-0241(2004)130:1(45).

Iskander, M., Chen, Z.B., Omidvar, M. and Guzman, I. (2013), "Rankine pseudo-static earth pressure for c-phi soils", *Mech. Res. Commun.*, **51**, 51-55. http://doi.org/10.1016/j.mechrescom.2013.04.010.

Karray, M., Hussien, M.N., Delisle, M.C. and Ledoux, C. (2018), "Framework to assess pseudo-static approach for seismic stability of clayey slopes", *Can. Geotech. J.*, **55**(12), 1860-1876. https://doi.org/10.1139/cgj-2017-0383.

Lee, M.G., Ha, J.G., Jo, S.B., Park, H.J. and Kim, D.S. (2017), "Assessment of horizontal seismic coefficient for gravity quay walls by centrifuge tests" *Geotech. Lett.*, **7**(2), 211-217. http://doi.org/10.1680/jgele.17.00005.

Lee, J., Liu, Q. and Park, H.J. (2019), "Effect of earthquake motion on the permanent displacement of embankment slopes", *KSCE J. Civ. Eng.*, **23**(10), 4174-4189. http://doi.org/10.1007/s12205-019-1833-0.

Lin, Y.L., Cheng, X.M., Yang, G.L. and Li, Y. (2018), "Seismic response of a sheet-pile wall with anchoring frame beam by numerical simulation and shaking table test", *Soil Dyn. Earthq. Eng.*, **115**, 352-364. http://doi.org/10.1016/j.soildyn.2018.07.028.

Lin, Y.L., Li, Y.X., Yang, G.L. and Li, Y. (2017a), "Experimental and numerical study on the seismic behavior of anchoring frame beam supporting soil slope on rock mass", *Soil Dyn. Earthq. Eng.*, **98**, 12-23. http://doi.org/10.1016/j.soildyn.2017.04.008.

Lin, Y.L., Li, Y.X., Zhao, L.H. and Yang, T.Y. (2020a), "Investigation on the seismic response of a three-stage soil slope supported by the anchor frame structure", *J. Cent. South Univ.*, **27**(4), 1290-1305. http://doi.org/10.1007/s11771-020-4367-1.

Lin, Y.L., Lu, L. and Yang, G.L. (2020b), "Seismic behavior of a single-form lattice anchoring structure and a combined retaining structure supporting soil slope: A comparison", *Environ. Earth Sci.*, **79**(3), 78. https://doi.org/10.1007/s12665-020-8817-8.

Lin, Y.L., Yang, G.L., Yang, X., Zhao, L.H., Shen, Q. and Qiu, M.M. (2017b), "Response of gravity retaining wall with anchoring frame beam supporting a steep rock slope subjected to earthquake loading", *Soil Dyn. Earthq. Eng.*, **92**, 633-649. http://doi.org/10.1016/j.soildyn.2016.11.002.

Lin, Y.L., Zhao, L.H., Yang, T.Y., Yang, G.L. and Chen X.B.

(2020c), "Investigation on seismic behavior of combined retaining structure with different rock shapes", *Struct. Eng. Mech.*, **73**(5), 599-612. http://doi.org/10.12989/sem.2020.73.5.599.

Ling, H.I., Leshchinsky, D., Wang, J.P., Mohri, Y. and Rosen, A. (2009), "Seismic response of geocell retaining walls: Experimental studies", *J. Geotech. Geoenviron. Eng.*, **135**(4), 515-524. https://doi.org/10.1061/(ASCE)1090-0241(2009)135:4(515).

Motlagh, A.T., Ghanbari, A., Maedeh, P.A. and Wu, W. (2018), "A new analytical approach to estimate the seismic tensile force of geosynthetic reinforcement respect to the uniform surcharge of slopes", *Earthq. Struct.*, **15**(6), 687-699. https://doi.org/10.12989/eas.2018.15.6.687.

Nian, T.K., Jiang, J.C., Wang, F.W., Yang, Q. and Luan, M.T. (2016), "Seismic stability analysis of slope reinforced with a row of piles", *Soil Dyn. Earthq. Eng.*, **84**, 83-93. https://doi.org/10.1016/j.soildyn.2016.01.023.

Nouri, H., Fakher, A. and Jones, C.J.F.P. (2008), "Evaluating the effects of the magnitude and amplification of pseudo-static acceleration on reinforced soil slopes and walls using the limit equilibrium horizontal slices method", *Geotext. Geomembranes,* **26**(3), 263-278. https://doi.org/10.1016/j.geotexmem.2007.09.002.

Ranjbar, K.A., Ganjian, N. and Askari, F.J. (2019), "Pseudo-static analysis of cantilever retaining walls using upper bound limit analysis approach", *J. Cent. South Univ.*, **26**(1), 241-255. https://doi.org/10.1007/s11771-019-3997-7.

Shi, K.Y., Wu, X.P., Liu, Z. and Dai, S.L. (2019), "Coupled calculation model for anchoring force loss in a slope reinforced by a frame beam and anchor cables", *Eng. Geol.*, **260**, 105245. http://doi.org/10.1016/j.enggeo.2019.105245.

Stamatopoulos, C.A., Bassanou, M., Brennan, A.J. and Madabhushi, G. (2007), "Mitigation of the seismic motion near the edge of cliff-type topographies", *Soil Dyn. Earthq. Eng.*, **27**(12), 1082-1100. http://doi.org/10.1016/j.soildyn.2007.01.012.

Stamatopoulos, C.A. and Bassanou, M. (2009), "Mitigation of the seismic motion near the edge of cliff-type topographies using anchors and piles", *B. Earthq. Eng.*, **7**(1), 221-253. http://doi.org/10.1007/s10518-008-9099-9.

Steedman, R.S. and Zeng, X. (1990), "The influence of phase on the calculation of pseudo-static earth pressure on a retaining wall", *Geotechnique,* **40**(1), 103-112. http://doi.org/10.1016/0148-9062(90)93144-B.

Takaji, K. (2019). "Energy-based Newmark method for earthquake-induced slope displacements", *Soil Dyn. Earthq. Eng.*, **121**, 121-134. http://doi.org/10.1016/j.soildyn.2019.02.027.

Xie, S., Gao, M., Chen, D., Sun, Y., Pan, H., Su, H. and Lan, S. (2018), "Stability influence factors analysis and construction of a deep beam anchorage structure in roadway roof", *Int. J. Min. Sci. Tech.*, **28**(3), 445-451. http://doi.org/10.1016/j.ijmst.2017.11.007.

Yan, M., Xia, Y., Liu, T. and Bowa, V.M. (2019), "Limit analysis under seismic conditions of a slope reinforced with prestressed anchor cables", *Comput. Geotech.*, **108**, 226-233. http://doi.org/10.1016/j.compgeo.2018.12.027.

Yan, X. and Liang, L. (2019), "Fatigue performance of post-installed anchorage beams", *Constr. Build. Mater.*, **229**, 116597. http://doi.org/10.1016/j.conbuildmat.2019.07.323.

Yazdandoust, M. (2017), "Investigation on the seismic performance of steel-strip reinforced-soil retaining walls using shaking table test", *Soil Dyn. Earthq. Eng.*, **97**, 216-232. https://doi.org/10.1016/j.soildyn.2017.03.011.

Yazdandoust, M. (2019a), "Assessment of horizontal seismic coefficient for three different types of reinforced soil structure using physical and analytical modeling", *Int. J. Geomech.*, **19**(7), 04019070. http://doi.org/10.1061/(ASCE)GM.1943-5622.0001344.

Yazdandoust, M. (2019b), "Shaking table modeling of MSE/soil nail hybrid retaining walls", *Soils Found.*, **59**(2), 241-252. https://doi.org/10.1016/j.sandf.2018.05.013.

Zamiran, S. and Osouli, A. (2018), "Seismic motion response and fragility analyses of cantilever retaining walls with cohesive backfill", *Soils Found.*, **58**(2), 412-426. http://doi.org/10.1016/j.sandf.2018.02.010.

Zhao, X.Y., Salgado, R. and Prezzi, M. (2014), "Centrifuge modelling of combined anchors for slope stability", *P. I. Civ. Eng. Geotech.*, **167**(4), 357-370. https://doi.org/10.1680/geng.12.00076.

Zhu, D.Y., Lee, C.F., Chan, D.H. and Jiang, H.D. (2005), "Evaluation of the stability of anchor-reinforced slopes", *Can. Geotech. J.*, **42**(5), 1342-1349. https://doi.org/10.1139/t05-060.

GC

Appendix 1: Expressions of f_n (n=0, 1, 2, ..., 6)

$$f_0=\frac{1}{3(1+9\tan^2\varphi)}\left[(3\tan\varphi\cdot\cos\theta_h+\sin\theta_h)\cdot e^{3(\theta-\theta_0)\tan\varphi}-(3\tan\varphi\cdot\cos\theta_0+\sin\theta_0)\right] \tag{20}$$

$$f_1=\frac{L}{6R_0}(2\cos\theta_0-\frac{L}{R_0})\cdot\sin\theta_0 \tag{21}$$

$$f_2=\frac{\alpha_3 H}{2R_0}\left[\cos^2\theta_0+\frac{L}{R_0}(\frac{L}{R_0}-2\cos\theta_0-\sin\theta_0\cot\beta_3)+\frac{1}{2}\sin 2\theta_0\cot\beta_3 -\frac{\alpha_3 H}{2R_0}\cdot\cot\beta_3\cdot(\cos\theta_0-\frac{L}{R_0}+\sin\theta_0\cot\beta_3)\right] \tag{22}$$

$$f_3=\frac{d_2}{3R_0}(\cos\theta_0-\frac{L}{R_0}-\alpha_3 H\cot\beta_3-\frac{d_2}{2R_0})(\sin\theta_0+\alpha_3\frac{H}{R_0}) \tag{23}$$

$$f_4=\frac{\alpha_1}{3}\cdot\frac{H}{R_0}\left[\cos^2\theta_0+\frac{L}{R_0}(\frac{L}{R_0}-2\cos\theta_0)+\sin\theta_0\cot\beta_2\cdot(\cos\theta_0-\frac{L}{R_0}-\frac{H}{R_0}\cdot\alpha_3\cot\beta_3-\frac{d_2}{R_0}) -\frac{\alpha_2}{2}\cdot\frac{H}{R_0}\cdot\cot\beta_2(\cos\theta_0-\frac{L}{R_0}+\sin\theta_0\cot\beta_2)-\alpha_3\cdot\frac{H}{R_0}\cdot\cot\beta_3(\cos\theta_0-\frac{L}{R_0})-2\cdot\frac{d_2}{R_0}\cdot(\cos\theta_0-\frac{L}{R_0})\right] \tag{24}$$

$$f_5=\frac{1}{3}\cdot\frac{d_1}{R_0}\left[\alpha_2\cdot\frac{H}{R_0}\cdot(\cos\theta_0-\frac{L}{R_0}-\alpha_2\cdot\frac{H}{R_0}\cdot\cot\beta_2-\alpha_3\frac{H}{R_0}\cdot\cot\beta_3-\sin\theta_0\cot\beta_3-\frac{1}{2}\cdot\frac{d_1}{R_0}-\frac{d_2}{R_0}) +\alpha_3\cdot\frac{H}{R_0}\cdot(\cos\theta_0-\frac{L}{R_0}-\alpha_2\cdot\frac{H}{R_0}\cdot\cot\beta_2-\alpha_3\frac{H}{R_0}\cdot\cot\beta_3-\sin\theta_0\cot\beta_3-\frac{1}{2}\cdot\frac{d_1}{R_0}-\frac{d_2}{R_0}) -\frac{L}{R_0}\cdot\sin\theta_0+\frac{1}{2}\sin\theta_0-\frac{1}{2}\cdot\frac{d_1}{R_0}\cdot\sin\theta_0-2\cdot\frac{d_2}{R_0}\cdot\sin\theta_0\right] \tag{25}$$

$$f_6=\frac{\alpha_1}{3}\cdot\frac{H}{R_0}\left[(\cos^2\theta_h+\frac{1}{2}\sin 2\theta_h\cot\beta_1)\cdot e^{2(\theta_h-\theta_0)\tan\varphi}+\frac{\alpha_1}{2}\cdot\frac{H}{R_0}\cdot\cot\beta_1(\cos\theta_h+\sin\theta_h\cot\beta_1)\cdot e^{(\theta_h-\theta_0)\tan\varphi}\right] \tag{26}$$

Appendix 2: Expressions of g_n (n=0, 1, 2, ..., 6)

$$g_0=\frac{1}{3(1+9\tan^2\varphi)}\left[(3\tan\varphi\cdot\sin\theta_h-\cos\theta_h)\cdot e^{3(\theta-\theta_0)\tan\varphi}-(3\tan\varphi\cdot\sin\theta_0-\cos\theta_0)\right] \tag{27}$$

$$g_1=\frac{1}{3}\cdot\frac{L}{R_0}\cdot\sin^2\theta_0 \tag{28}$$

$$g_2=\frac{\alpha_3 H}{3R_0}\left[\cot\beta_3\sin^2\theta_0+\frac{1}{2}\sin 2\theta_0-\frac{L}{R_0}\cdot\sin\theta_0+\frac{\alpha_3 H}{2R_0}\cdot\cot\beta_3\cdot(\cos\theta_0-\frac{L}{R_0}+\sin\theta_0\cot\beta_3)\right] \tag{29}$$

$$g_3=\frac{d_2}{3R_0}(\sin\theta_0+\alpha_3\frac{H}{R_0})^2 \tag{30}$$

$$g_4=\frac{\alpha_3}{3}\cdot\frac{H}{R_0}\left[\cot\beta_2\sin^2\theta_0+\frac{1}{2}\sin 2\theta_0-\frac{L}{R_0}\cdot\sin\theta_0-\frac{\alpha_2}{2}\cdot\frac{H}{R_0}\cdot\cot\beta_2(\cos\theta_0-\frac{L}{R_0}+\sin\theta_0\cot\beta_2) -\alpha_3\cdot\frac{H}{R_0}(\cos\theta_0-\frac{L}{R_0}+\sin\theta_0\cot\beta_2)-\frac{d_2}{R_0}\cdot(\frac{\alpha_2 H}{2R_0}+\alpha_3\frac{H}{R_0}+\sin\theta_0)\right] \tag{31}$$

$$g_5=\frac{1}{3}\cdot\frac{d_1}{R_0}\left[(\alpha_2+\alpha_3)\cdot\frac{H}{R_0}+\sin\theta_0\right]^2 \tag{32}$$

$$g_6=\frac{\alpha_1}{3}\cdot\frac{H}{R_0}\left[\sin\theta_h\cdot e^{(\theta_h-\theta_0)\tan\varphi}-\frac{\alpha_1}{2}\cdot\frac{H}{R_0}\right]\cdot(\cos\theta_h+\sin\theta_h\cot\beta_1)\cdot e^{2(\theta_h-\theta_0)\tan\varphi} \tag{33}$$